

Influence of thermal process parameters on the properties of material jetted CuSn8 components

Maximilian Ploetz, Benedikt Kirchebner, Wolfram Volk, Philipp Lechner

Angaben zur Veröffentlichung / Publication details:

Ploetz, Maximilian, Benedikt Kirchebner, Wolfram Volk, and Philipp Lechner. 2023. "Influence of thermal process parameters on the properties of material jetted CuSn8 components." *Materials Science and Engineering: A* 871: 144869. <https://doi.org/10.1016/j.msea.2023.144869>.

Influence of thermal process parameters on the properties of material jetted CuSn8 components

Maximilian Ploetz*, Benedikt Kirchebner, Wolfram Volk, Philipp Lechner

Chair of Metal Forming and Casting, TUM School of Engineering and Design, Technical University of Munich, Walther-Meissner-Str. 4, 85748 Garching, Germany

1. Introduction

Copper and its alloys are widely used as described by Warlimont and Martiensse [1] due to their high electrical and thermal conductivity combined with favourable mechanical and corrosion resistant properties. They are therefore an indispensable material for many branches of industry. According to Davis [2], pure copper is often used for applications with high electrical and/or thermal conductivity requirements, such as heat exchangers or electrical conductors. In comparison, copper–tin–bronzes have significantly lower thermal and electrical conductivity. Nevertheless, the addition of tin improves the mechanical strength and hardness compared to pure copper. Leygraf et al. [3] also notes that the addition of tin usually improves corrosion resistance. Bronze can be used for high precision springs and bearings, as Alavudeen et al. [4] mentioned. In addition, Kadhim and Abed [5] shows that it can be used in applications in corrosive environments. Due to the different properties of pure copper and copper–tin–bronze, the combination of the two materials in one component is a promising

approach for the production of topology-optimized components. The production of composite components made of copper and bronze using a composite casting process has already been demonstrated by Mittler et al. [6].

If components with particularly complex geometries are required, they are often difficult to produce using conventional manufacturing processes, as Constantin et al. [7] mention. In addition, the cost-effective production of small batches or prototypes can be a problem for conventional manufacturing processes. Additive manufacturing processes can be a possible alternative here.

As shown by Jiang et al. [8], powder bed fusion (PBF) processes currently dominate additive manufacturing of copper materials components. According to Körner [9], the cohesion of the powder can be achieved by melting and solidification, as is done in selective laser melting (SLM) or selective electron beam melting (SEBM). In addition to melting and solidification, cohesion can also be achieved by the local addition of binders to the powder bed, which is cured in a further

* Corresponding author.

E-mail address: maximilian.ploetz@utg.de (M. Ploetz).

step. This so-called binder jetting process (BJT) is shown by Bai and Williams [10] for copper. In addition to PBF, other processes such as laser powder deposition as demonstrated by Oniuke et al. [11], cold spray as showed by Huang et al. [12] or fused deposition modeling as used by Dehdari Ebrahimi and Ju [13] exist for additive processing of copper materials. With some of the AM processes mentioned above, it has already been possible to manufacture multi-material components from copper and other materials, as Bai et al. [14] and Liu et al. [15] have shown, for example.

However, the processing of copper materials and the production of multi-material components pose a challenge for the currently established AM processes. A key challenge in additive processing of copper materials in SLM is according to Lingqin et al. [16] the low absorption coefficient of the copper material compared to the currently commercially available lasers and the high thermal conductivity. As shown in the work of Jadhav et al. [17], the reflections that occur can cause damage to the optics. According to Jiang et al. [8], no unwanted reflections occur with SEBM. Gokuldoss et al. [18], however, states that the application of the method is limited due to the high cost of the required equipment. Also in BJT, the absorption behavior has no influence due to the solidification of the powder by binders. However, Jiang et al. [8] mentions that the components produced in BJT have lower density and significantly lower strength. In addition, powder recycling is a major challenge in the economical production of components using PBF processes, as Gorji et al. [19] mentions. Particularly in the manufacture of multi-material components, powder recycling presents a challenge, as Horn et al. [20] describes, because a mixture of powders is present after manufacture.

The material jetting process (MJT) offers the possibility for overcoming such disadvantages, since no powdered semi-finished material or laser is required. Following Wohlers et al. [21], in the MJT process the build material is melted in a print head and applied dropwise to a build platform. Previous investigations of the MJT process with metallic materials have mostly been limited to those materials with a melting point of that of aluminum or below. Initial investigations into the fabrication of aluminum components were conducted by Orme and Smith [22]. Fang et al. [23] used parametric studies to investigate heat transfer during the printing of aluminum columns. It was shown that for good droplet adhesion, the temperature of the top droplet must be close to the melting temperature of the building material. The quality of droplet adhesion has a significant influence on the mechanical properties of the printed components. This relationship was also investigated by Zuo et al. [24] when they studied the influence of different droplet and build platform temperatures on droplet bonding. It was possible to produce components with strengths comparable to extruded specimens. Further studies on the influence of pressure parameters on the process were carried out by Cao and Miyamoto [25] and Aziz and Chandra [26]. To realize overhangs, Kirchebner et al. [27] investigated the MJT of water-soluble salt support structures. Studies on the processing of copper materials with a pneumatic print head were carried out by Zhong et al. [28]. Parameter studies were conducted on the influence of parameters during droplet generation. Droplets could be generated at pressures of 30 kPa and 35 kPa and valve opening times between 600 μ s and 900 μ s. An increase in droplet diameter was observed with increasing pressure. In further experiments, Zhong et al. [29] again investigated the influences during droplet formation and compared the results with simulations.

1.1. Research goal

The ultimate goal of this research is to enable the material jetting of multi-material copper-bronze components that combine the strength of bronze and the conductivity of pure copper. As a first step, we analyzed the processing and achievable mechanical properties of copper-tin-bronze components.

In the processing of aluminum alloys, it is well known that the properties of the printed components depend significantly on the thermal process conditions during droplet deposition. In this article we investigate the processability of copper-tin-bronze in the MJT process. This leads to the research question: "What influence do the thermal process variables droplet temperature and build platform temperature have on the quality of copper-tin-bronze components produced in the MJT process?"

To answer the research question, the following hypotheses will be tested:

- Both droplet and build platform temperatures have an effect on the properties of copper-tin-bronze components produced in the MJT process.
- The build platform temperature has a stronger influence on the quality of the printed components than does the droplet temperature.
- The relative component density increases with increasing build platform and droplet temperature.
- Increasing the build platform and droplet temperature can increase the strength and tolerable strains of the printed parts.

To answer the research question, the hypotheses are tested by characterising copper-tin-bronze test specimens produced in the MJT process. The mechanical characterization is performed by uniaxial tensile tests. In addition, an optical examination of the component and the fracture surface will be performed. Micrographs are used to investigate the droplet bonding and to determine the relative component density.

2. Materials and methods

2.1. Setup

2.1.1. Test stand for MJT with copper alloys

Fig. 1 shows a schematic of the test stand used for the production of the test specimens. This is essentially based on the system described by Himmel et al. [30], which was originally developed for processing aluminum materials. The test stand consists of a process chamber flooded with nitrogen and containing a build platform that can be moved in the horizontal and vertical directions. A print head can be placed on the process chamber to create droplets of the build material. To be able to provide the temperatures required for processing copper materials, a new print head was developed and integrated into the system. In addition, the existing build platform was replaced by a newly developed build platform to be able to realize higher build platform temperatures.

In the center of the printhead there is a cylindrical crucible made of graphite in which the wire-shaped semi-finished product is melted and the melt is stored. The crucible is heated by two heating elements placed on the side of the crucible. At the bottom, the crucible is closed with a nozzle made of graphite. The borehole of the nozzles is chosen small enough (500 μ m) that no melt escapes when the system is at rest. CuSn8 droplets can be dispensed through the nozzle orifice by a pneumatic pressure surge acting on the melt. The amount of material dispensed is replaced during the process by feeding wire-shaped semi-finished material into the crucible. This keeps the melt level in the crucible constant. The droplets are generated according to the drop-on-demand principle. The duration and pressure level of the pulse can be specified via the system control. As process gas for droplet generation, nitrogen is used. In addition, the area around the crucible and the nozzle is flooded with nitrogen to reduce thermal wear on the components. Insulating components are installed in the printhead to reduce heat loss to the environment. The movable build platform is located below the static printhead in the process chamber. A ceramic heating element is installed in the build platform. This allows the build platform to be heated to a maximum temperature of 1020 °C. A 1.5 mm thick stainless steel plate is placed on the build platform as a substrate plate onto which the droplets are deposited.

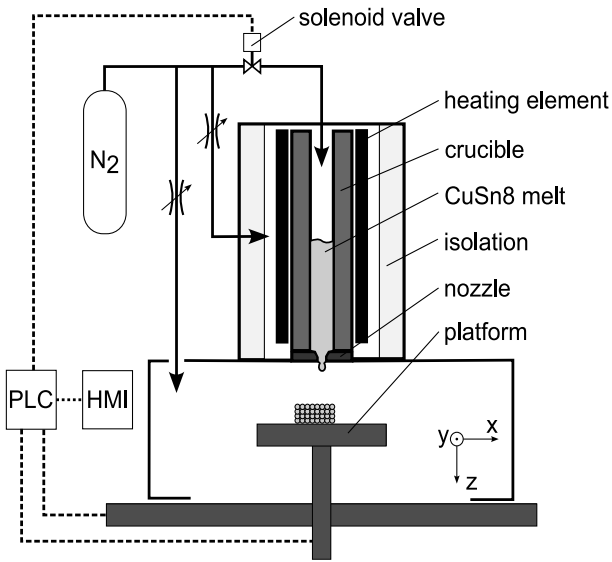


Fig. 1. Schematic view of the MJT test stand for copper melts according to Kirchebner et al. [27]. The test stand consists of a nitrogen purged process chamber onto which the printhead is placed. The process chamber contains a movable build platform onto which the droplets generated by the printhead are deposited. The area of the building platform that can be used for production is 60 mm × 60 mm. In the z-direction, the build platform can be moved down by 80 mm relative to the bottom of the printhead.

2.1.2. Experimental setup

The images for the optical microscopy of the component surfaces are taken with the digital microscope (VHX-2000, Keyence Deutschland GmbH, Neu-Isenburg, Germany). The VH-Z20R objective used allows magnification between 20:1 and 200:1. The micrographs for metallography were acquired with the AxioCam MRC5 camera system. This is part of the reflected light microscope (Axioplan 2, Carl Zeiss MicroImaging GmbH, Göttingen, Germany). The determination of the relative component density based on the micrographs is done with the open-source image processing software Fiji described by Schindelin et al. [31]. A precision balance (PCB250-3, KERN & Sohn GmbH, Balingen, Germany) is used to determine the relative component density according to the Archimedean principle. A universal testing machine (1484/DUPS-M, Zwick GmbH & Co. KG, Ulm, Germany) is used to perform a quasi-static tensile test. Strain is measured with an extensometer (makro, Zwick GmbH & Co. KG, Ulm, Germany). A scanning electron microscope (JSM-7500F, JEOL (Deutschland) GmbH, Freising, Germany) is used to record the fracture surfaces generated in the tensile test.

2.2. Sample description

2.2.1. Build material

The material CuSn8 is used as the built material for all test specimens. It is a copper–tin–bronze with a tin content of 8%. The semi-finished product is in the form of wire with a diameter of 2 mm (Wieland-Werke AG, Ulm, Germany). The copper alloy has a liquidus temperature of 1040 °C and a solidus temperature of 860 °C. The chemical composition of a printed sample was determined using a spark spectrometer (FOUNDRY-MASTER, Worldwide Analytical Systems GmbH, Kleve, Germany). The three elements with the highest concentrations are listed in Table 1. Besides the main alloying element tin, phosphorus is mainly present.

2.2.2. Geometrie and printing strategy

For the analysis of the printing process, cuboid samples with a base area of approx. 41 mm × 6.5 mm are printed. The height of the cuboids varies between 5.5 mm and 7.6 mm depending on the process parameters

Table 1

Composition of a material jetted CuSn8 sample as determined by optical emission spectroscopy. All values in %.

Element	Average concentration	Concentration in measurement 1	Concentration in measurement 2	Concentration in measurement 3
Cu	92.9	92.9	92.9	92.8
Sn	7.04	7.00	7.05	7.08
P	0.0226	0.0227	0.0234	0.0218

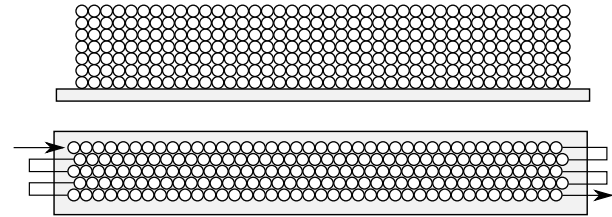


Fig. 2. Specimen geometry and printing strategy. The top line shows a principle sketch of the side view of a cuboid printed on the substrate plate. The bottom line shows the top view of the cuboid. The printing strategy is illustrated by the arrow.

Table 2

Overview of the process parameters used. For the droplet and build platform temperatures, three stages each were investigated in a full factorial design. The droplet diameter, the pressure frequency and the residual oxygen content prevailing in the process chamber were kept constant during the printing of the samples.

Parameter	Symol	Values
Temperature droplet	T_{droplet}	1090 °C
		1140 °C
		1190 °C
Temperature platform	T_{platform}	650 °C
		750 °C
		850 °C
Droplet diameter	d_{droplet}	1.1 mm
Deposition rate	$f_{\text{deposition}}$	15 Hz
Oxygen in chamber	c_{O_2}	<50 ppm

used. Each cuboid consists of seven layers with 200 droplets each. To create a layer, five parallel lines with 40 droplets each are printed. The distance between the lines is 1.1 mm. Within a line, the build platform moves between the deposition of each droplet by a distance of 1 mm. The lines of a layer are arranged so that the deposition of the droplets is offset by half a droplet diameter. In Fig. 2 the geometry of a cuboid and the printing strategy are shown schematically. The top line shows a principle sketch of the side view of a cuboid printed on the substrate plate. The bottom line shows the top view of the cuboid and the printing strategy illustrated by the arrow.

2.3. Experimental procedure

Fig. 3 shows the sample preparation procedure and the investigation methods used to characterize the components.

In a first step, the cuboid test specimens are manufactured in the MJT process on the previously presented MJT test stand. The process parameters listed in Table 2 are used to manufacture the specimens.

For droplet and build platform temperatures, three levels each were investigated in a full factorial design. The droplet temperature was set at $T_{\text{droplet}} = 1090$ °C, $T_{\text{droplet}} = 1140$ °C, and $T_{\text{droplet}} = 1190$ °C. The lowest droplet temperature investigated is thus 50 °C above the liquidus temperature of the copper–tin–bronze. In addition, the other two temperatures are investigated to increase the thermal energy introduced by the droplet. The build platform temperatures to be investigated are $T_{\text{platform}} = 650$ °C, $T_{\text{platform}} = 750$ °C and $T_{\text{platform}} = 850$ °C. The temperatures reached in the substrate are about 70 K lower than those set on the build platform. The maximum substrate temperature selected must be below the solidus temperature of the copper–tin–bronze so that

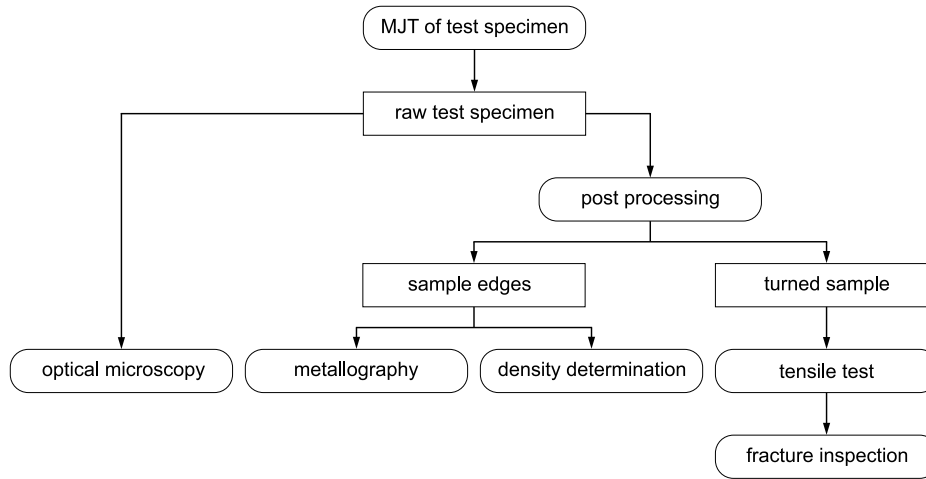


Fig. 3. Flow chart of experimental procedure. Optical microscopy, metallography, density determination, tensile test and fracture inspection are performed to examine the samples.

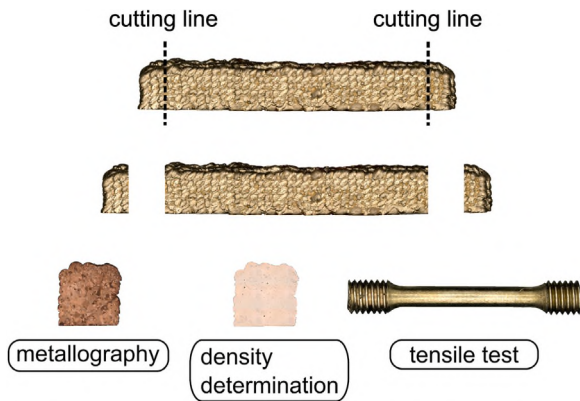


Fig. 4. Post-processing methods. The ends of the specimens are cut off by machining and embedded in resin. A round tensile specimen is made from the center piece of the specimen.

the component already produced does not melt again. Therefore, the maximum temperature of the build platform is set at $T_{\text{platform}} = 850\text{ }^{\circ}\text{C}$. In order to obtain a faster solidification of the droplet, the two other temperatures are chosen. During a printing process, two components, which are placed centrally on the build platform are printed. This minimizes the influence of a temperature gradient in the build platform. The generated droplets have a diameter of 1.1 mm and are deposited on the build platform at a frequency of 15 Hz. During the printing process, the residual oxygen content in the process chamber is less than 50 ppm. After the printing process, the component surface is optically inspected. The printed cuboids are then forwarded for post-processing. In this step, the ends of the cuboids are cut off by machining. Fig. 4 illustrates this process. The edge pieces are embedded in epoxy resin (KulzerGmbH, Hanau, Germany), ground and polished. The unetched ground specimens are used to determine the relative component density. For metallographic characterization, the specimens are etched. Round tensile specimens are made from the center portion of the printed cuboid. Mechanical characterization is performed using tensile tests. The fracture surfaces produced in the tensile test are finally examined by scanning electron microscopy.

The following chapters describe the procedure for carrying out the individual characterization methods.

2.3.1. Optical microscopy

Optical microscopy is used to examine the surface of the produced components at various parameters. This allows conclusions to be drawn

about possible geometric deviations from the cuboid target geometry due to the printing process. In addition, the components are evaluated with regard to possible open porosity. For each parameter configuration, all surfaces of the four printed components are photographed with the digital microscope. In order to compare the components, one image of a characteristic part is used in this work for each parameter configuration. The front view of the cuboid samples is chosen as the comparison view in each case. The images are also used to determine the height of the component. The measurement is done in the middle of each component. For the determination of the component height, the four manufactured components are used for each parameter configuration.

2.3.2. Density determination

As no standardized method for determining the relative density of components manufactured using the MJT process is available to date, the determination is based on the method of VDI 3405–2, which relates to additively manufactured metal components using the beam melting process. The relative component density can be determined from the unetched micrographs by means of image analysis. The suitability of this method has already been demonstrated by Himmel et al. [32] for aluminum components manufactured by the MJT process. For each parameter configuration, the two ends of the four components are used, resulting in a total number of eight samples per parameter configuration. Comparison of relative component densities is performed using the calculated mean values. Since the relative component density determined from the micrographs produced depends strongly on the selected position of the specimen, an additional density determination was carried out using Archimedes' principle. This method is also recommended in VDI 3405–2. The tensile specimens produced by machining are used as test specimens. The tendency of the results is identical for both test methods, which is why the relative component densities determined from the micrographs prepared are presented below.

2.3.3. Metallography

The material microstructure and droplet bonding are studied using the embedded ends of the samples previously used to determine the relative component density. For this purpose, the polished sample surface is etched with ferric chloride for 15 s. The sample is then examined using the Axioplan 2 reflected light microscope. In order to compare the components printed at different parameters, a characteristic component is again selected for each parameter configuration. The grain size is also determined using the reflected light microscope according to the procedure defined in ASTM E 112 - 13. For the determination of the average grain size, one component per parameter configuration was used and three measurements per component were carried out.

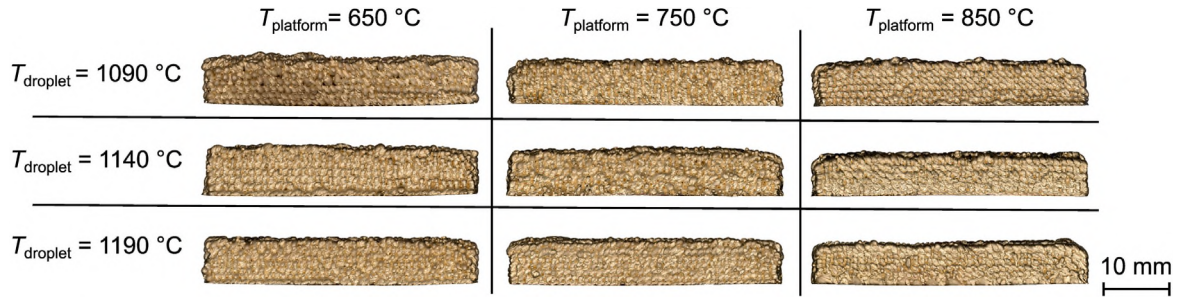


Fig. 5. Optical examination of the component surfaces. The figure shows the surfaces of the cuboids in the side view. With increasing temperature of the build platform, a decrease in the component height can be observed. In addition, the pores visible on the surface decrease.

2.3.4. Tensile test

Quasi-static tensile tests with a strain rate of $2.5 \times 10^{-4} \text{ s}^{-1}$ are carried out to mechanically characterize the printed components. Round tensile specimens with a diameter of 3 mm and a parallel length of 18 mm are used as specimen geometry. Four specimens are tested for each parameter configuration. During the tensile test, the force-displacement curves, from which the tensile strength and uniform strain are determined for each specimen are recorded. Comparison of the specimens produced at different parameters is based on the arithmetic mean values of the determined characteristic values.

2.3.5. Fracture inspection

Following the tensile test, the resulting fracture surfaces are examined by scanning electron microscopy. Again, characteristic components are selected for the individual parameter configurations and the fracture surfaces are compared.

3. Results

In the following chapter, the results of the component characterization for the different investigation methods are presented.

3.1. Optical microscopy

Fig. 5 shows the side view of nine components printed at different droplet and build platform temperatures. Within one row of the matrix, the components shown were printed at the same droplet temperature. Within a row, the platform temperature increases from left to right. Within a column, the droplet temperature varies while the build platform temperature remains constant.

The cuboid geometry of the components is recognizable for all investigated build platform and droplet temperatures. The length and width dimensions do not differ for the various parameter configurations used and correspond to the specified geometry. However, a deviation can be seen in the height of the components. The values of the component height are shown in Fig. 6. In this figure the three investigated build platform temperatures are plotted on the abscissa. For each build platform temperature studied, the corresponding mean values of the component height produced at the three droplet temperatures studied are plotted. The corresponding error bars show the standard deviation based on four samples. A decrease in component height can be observed as the temperature of the build platform increases. A tendency with regard to the influence of the droplet temperature is not recognizable. The influence of the build platform temperature is more pronounced than the influence of the droplet temperature. The lowest component height is obtained for the specimen produced at a droplet temperature $T_{\text{droplet}} = 1190 \text{ °C}$ and a build platform temperature $T_{\text{platform}} = 850 \text{ °C}$.

In addition, a decrease in the number of pores visible on the component surface can be observed with increasing build platform and droplet temperature. Fig. 7 shows, on the left, the component surface of a component manufactured at $T_{\text{droplet}} = 1090 \text{ °C}$ and $T_{\text{platform}} = 650 \text{ °C}$.

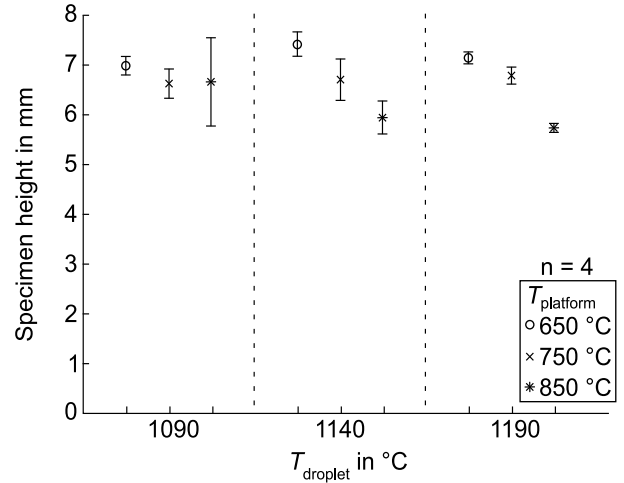


Fig. 6. Component height as a function of the droplet and platform temperatures investigated. With increasing droplet and platform temperatures, a decrease in component height tends to be observed.

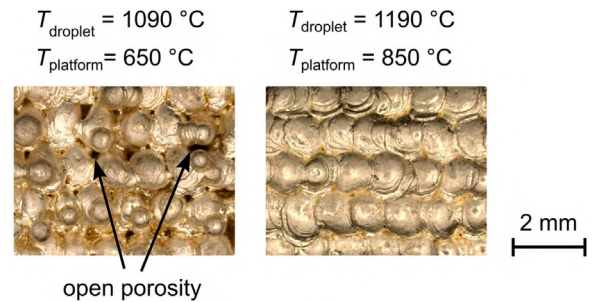


Fig. 7. Comparison of component surfaces. The left image shows the surface of the component produced at a $T_{\text{droplet}} = 1090 \text{ °C}$ and a $T_{\text{platform}} = 650 \text{ °C}$. Areas of open porosity can be seen in this component. The component shown on the right, which was printed at $T_{\text{droplet}} = 1190 \text{ °C}$ and a $T_{\text{platform}} = 850 \text{ °C}$, has a closed surface.

The right side shows the component surface of a component printed at $T_{\text{droplet}} = 1190 \text{ °C}$ and $T_{\text{platform}} = 850 \text{ °C}$. Both images show the top view of the cuboids.

The surface of the component on the left side of the image shows areas of open porosity over the entire surface of the component. As the temperature of the build platform or droplet increases, the surface becomes more uniform and fewer near-surface pores are visible. The surface of the component shown on the right side of the figure has no visible surface pores.

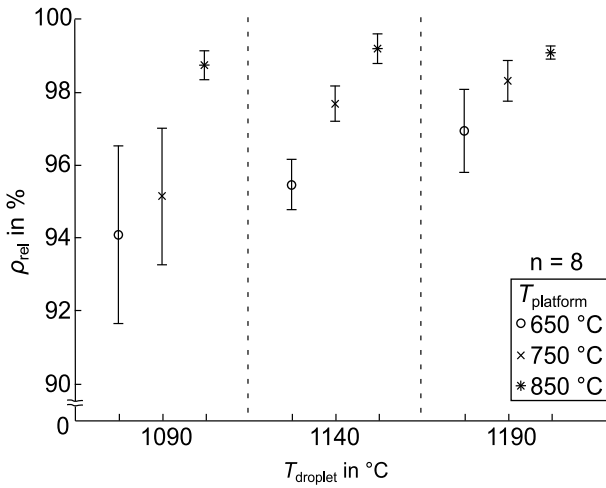


Fig. 8. Relative density values as a function of the droplet and platform temperatures investigated. An increase in relative density is observed with increasing droplet and platform temperature.

3.2. Density determination

In addition to evaluating the visually visible pores on the component surface, an evaluation of the porosity of the overall component will also be carried out. For this purpose, the relative density of the components produced at the three different build plate and droplet temperatures is compared below. Fig. 8 compares the relative component densities determined from the micrographs for the different droplet and build platform temperatures.

Within a group, an increase in relative component density is observed as a result of an increase in the temperature of the build platform. An increase in relative component density with increasing droplet temperature is also observed between groups. The lowest relative component density is obtained for the combination of the lowest droplet temperature studied $T_{\text{droplet}} = 1090$ °C and the lowest build platform temperature $T_{\text{platform}} = 650$ °C and is 94.1%. This parameter configuration also has the highest standard deviation value, indicating greater variation within the process compared to the other parameter configurations. The highest relative component densities are obtained for the components produced at the build platform temperature of $T_{\text{platform}} = 850$ °C. The highest relative component density is obtained at the parameter combination $T_{\text{droplet}} = 1140$ °C and $T_{\text{platform}} = 850$ °C and is 98.8%. The standard deviation of the relative component density is lowest for the components at a platform temperature $T_{\text{platform}} = 850$ °C. Moreover, at this build platform temperature, the achieved relative component densities for different droplet temperatures are insignificantly different from each other.

3.3. Metallography

In addition to the component density, the micrographs are used to analyze the material structure and droplet bonding. For this purpose, the embedded samples are etched as described. Fig. 9 shows nine etched micrographs of the cuboids for the droplet and build platform temperatures investigated.

With increasing droplet and build platform temperature, a decrease in the porosity prevailing in the component can be observed, as already described. In addition, an increase in grain size tends to be observed. The grain size number G according to ASTM E 112 - 13 is used to compare the grain size. The results are shown in Fig. 10.

The build platform temperature again has a more dominant influence on the change in material structure than does the droplet temperature. The components produced at lower temperatures have

smaller grain sizes and in some cases areas with a cast structure. Especially at the parameter configuration of $T_{\text{platform}} = 650$ °C and $T_{\text{droplet}} = 1090$ °C, the component shows a cast structure almost over the entire cross-section. As the temperature increases, only a few areas with a cast structure can be seen. These are mostly limited to the top layer of the component. In addition, at the lower build platform temperature, the individual droplets can be seen to some degree. There are areas where, despite material contact, there is no material connection between the droplets. In addition, micro shrinkage can be observed in the area of the interface between two droplets. The components produced at higher temperatures show a recrystallized structure over almost the entire cross-section. As the temperature of the building platform increases, a decrease in the grain size number G and thus an increase in the grain size can be observed. At the higher temperatures, the boundaries between the individual droplets are often no longer recognizable. Grain growth here occurs across the droplet boundaries. Epitaxy can be observed during this process. Epitaxy also takes place at low droplet and platform temperatures, but less frequently. Fig. 11 shows Epitaxy in the cast structure and the recrystallized structure.

3.4. Tensile test

In the following, the results of the mechanical characterization of the printed test specimens, which was carried out by means of uniaxial tensile tests are presented. In Fig. 12, the results of the uniaxial tensile test are presented. The arrangement of the results is analogous to the relative component density presented previously. For each parameter configuration, four specimens are examined.

Both an increase in the build plate temperature and an increase in the droplet temperature cause an increase in the determined tensile strength. The lowest tensile strength is obtained with a value of 103 MPa for the parameter configuration droplet temperature $T_{\text{droplet}} = 1090$ °C and build platform temperature $T_{\text{platform}} = 650$ °C. By increasing the build platform temperature to $T_{\text{platform}} = 850$ °C at the lowest droplet temperature selected of $T_{\text{droplet}} = 1090$ °C, the tensile strength was increased to 291 MPa. The highest component strength was obtained at the highest investigated process parameter combination of droplet temperature $T_{\text{droplet}} = 1190$ °C and build platform temperature $T_{\text{platform}} = 850$ °C. The strength at this parameter configuration is 330 MPa, which is about three times higher than at the lowest temperature combination.

Fig. 13 shows the uniform strain obtained in the tensile test. Analogous to the tensile strength values, an increase in the uniform strains achieved is observed with increasing droplet and platform temperature. The achieved values range from $A_g = 0.5\%$ for the parameter combination droplet temperature $T_{\text{droplet}} = 1090$ °C and build platform temperature $T_{\text{platform}} = 650$ °C to $A_g = 54.0\%$ at the selected droplet temperature $T_{\text{droplet}} = 1190$ °C and the build platform temperature $T_{\text{platform}} = 850$ °C. The more dominant influence of the build platform temperature on the printing result compared to the droplet temperature can be clearly seen in the uniform strain values. At the highest droplet temperature selected $T_{\text{droplet}} = 1190$ °C and the build platform temperature $T_{\text{platform}} = 650$ °C, the uniform strain value is 9.4%. In contrast, increasing the platform temperature to $T_{\text{platform}} = 850$ °C using the lowest droplet temperature $T_{\text{droplet}} = 1090$ °C leads to an increase in uniform strain to 33.2%.

3.5. Fracture inspection

Fig. 14 shows the fracture surfaces of three samples fabricated at different platform temperatures taken with the scanning electron microscope. For the fabrication of the specimens, the droplet temperature was set to $T_{\text{droplet}} = 1190$ °C. The build platform temperature is examined at the three levels presented.

As the temperature of the platform increases, the fracture surface exhibits an increasingly homogeneous structure. The fracture surface

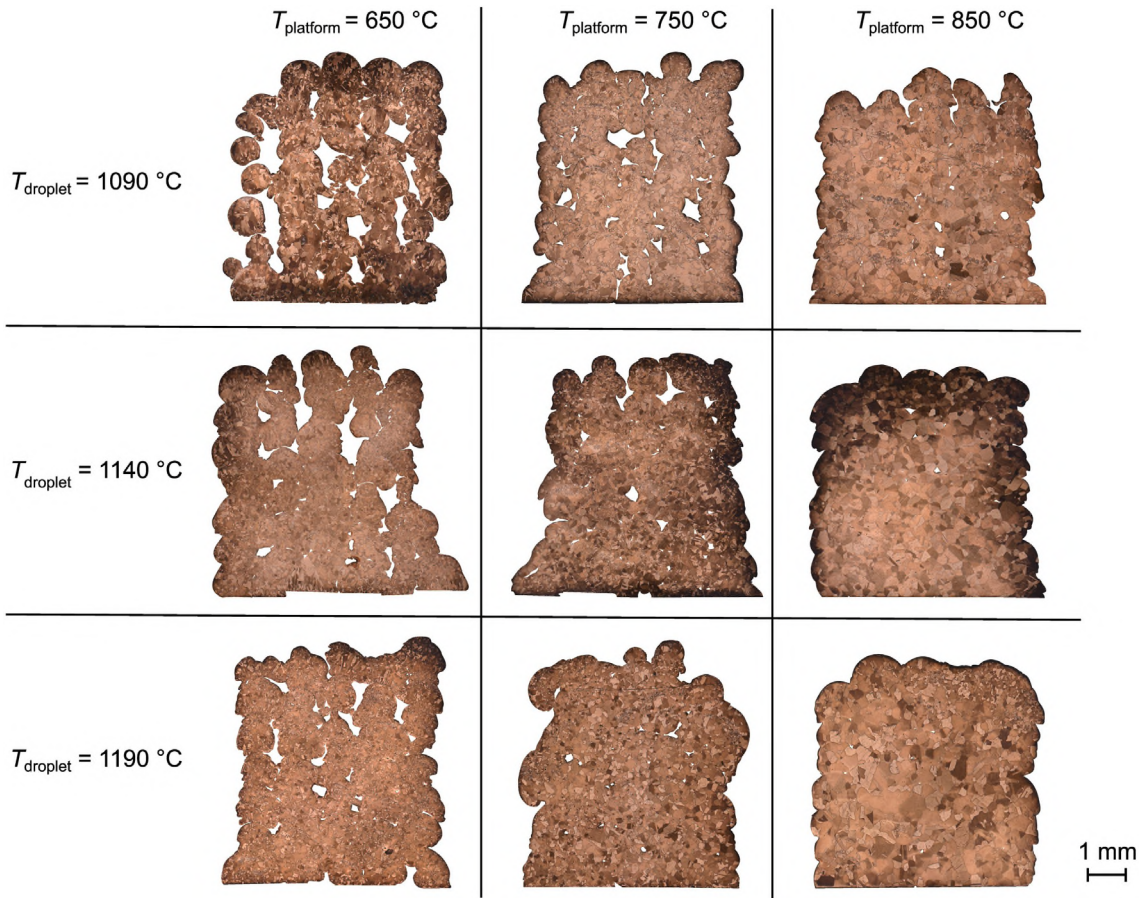


Fig. 9. Etched microphotographs of the printed samples. A decrease in porosity is observed with increasing droplet and build platform temperature. In addition, components produced at higher build platform temperatures exhibit larger grains. In some cases, grain growth occurs beyond the droplet boundaries.

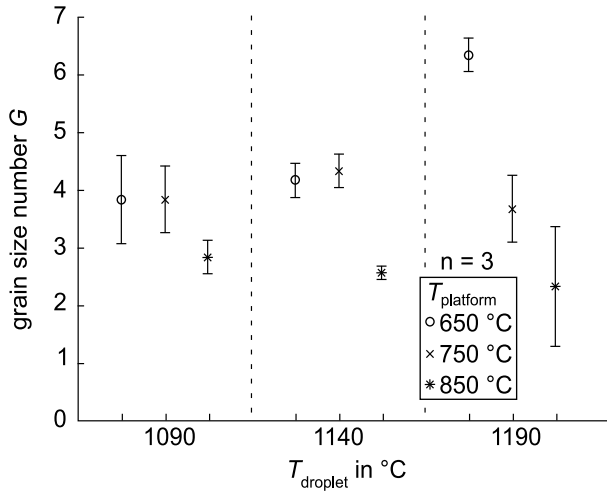


Fig. 10. Grain size number G as a function of the droplet and platform temperatures investigated. As the temperature of the building platform increases, the grain size tends to increase.

of the component shown on the left, which was produced at a build platform temperature of $T_{\text{platform}} = 650\text{ }^{\circ}\text{C}$, shows areas where the newly deposited droplets have not fused with the already deposited substrate. In these areas, the smooth, wavy surfaces of the droplets can be seen. Only in isolated areas, mostly at the top of the droplets, do the newly deposited droplets form a cohesive bond between the

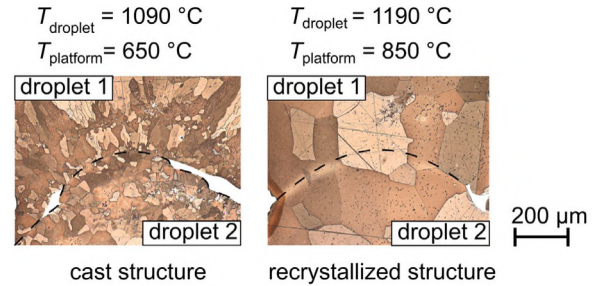


Fig. 11. Comparison of the material microstructure. The left image shows the microstructure of the component produced at a $T_{\text{droplet}} = 1090\text{ }^{\circ}\text{C}$ and a $T_{\text{platform}} = 650\text{ }^{\circ}\text{C}$. The component primarily has a cast structure. The component shown on the right, which was printed at $T_{\text{droplet}} = 1190\text{ }^{\circ}\text{C}$ and a $T_{\text{platform}} = 850\text{ }^{\circ}\text{C}$, has a recrystallized structure. Epitaxy occurs in both the cast and recrystallized structure.

droplets. These areas increase with increasing platform temperature. The fracture surface of the component shown on the right, which was produced at a droplet temperature of $T_{\text{platform}} = 850\text{ }^{\circ}\text{C}$, exhibits a honeycomb-like fracture surface almost over the entire cross section. Cohesive bonding of the droplets has occurred in these areas.

Fig. 15 shows the fracture surfaces of the components produced at constant build platform temperature $T_{\text{platform}} = 850\text{ }^{\circ}\text{C}$ at the three different droplet temperatures. At this build platform temperature, only a small effect of the droplet temperature on the expression of the material cohesion can be seen. For all specimens, a honeycomb-like fracture surface can be seen almost over the entire fracture surface. Especially at the build platform temperatures $T_{\text{platform}} = 650\text{ }^{\circ}\text{C}$ and

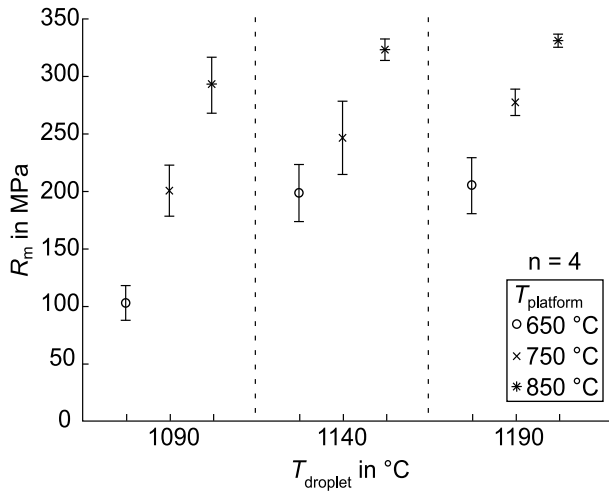


Fig. 12. Tensile strength values as a function of the droplet and platform temperatures investigated. An increase in tensile strength is observed with increasing droplet and platform temperature.

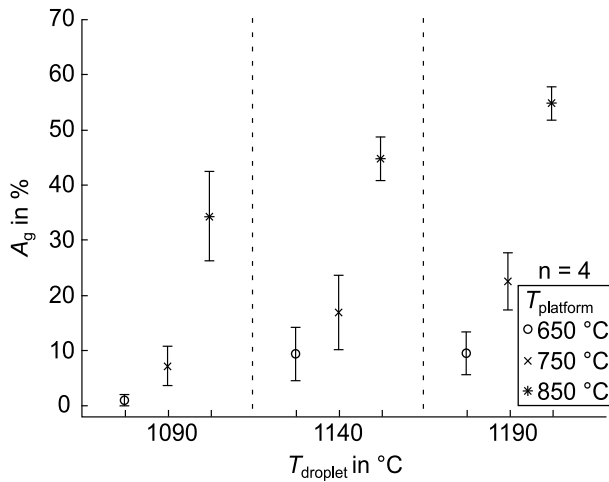


Fig. 13. Uniform elongation values as a function of the droplet and platform temperatures investigated. An increase in uniform elongation is observed with increasing droplet and platform temperature.

$T_{\text{platform}} = 750\text{ }^{\circ}\text{C}$, there are still areas where the smooth droplet surface can be observed. Due to the improved binding of the droplets, the sample contracts more before breakage of the sample occurs. As a result, a reduction in cross-section is observed. The wavy surface at the edge of the specimen cross-section is due to machining during post-processing.

4. Discussion

All the investigations carried out show that the droplet and build platform temperature have an influence on the component properties. An increase in the temperature in the contact area of the newly impinging droplets leads to an improvement in droplet adhesion for the parameters investigated. The increase in contact temperature can be achieved both by a higher droplet temperature and by a higher build platform temperature. The influence of the build platform temperature is more dominant than that of the droplet temperature. Higher build platform temperatures cause a permanent increase in temperatures

in the contact area. This temperature level cannot be achieved by increasing the droplet temperature. Higher droplet temperatures briefly increase the temperature in the contact area. However, due to the thermal conductivity of the copper material, the heat is quickly conducted to the rest of the component or the build plate and the environment. As a result, the contact temperature is lower compared to an increase in the temperature of the build platform.

Higher contact temperatures generally lead to better fusion of the newly deposited droplets with the substrate. Due to the higher temperatures, the newly deposited droplets penetrate the process-related unevenness of the already manufactured component. This reduces the pores in the material structure, which increases the relative component density. In addition, local melting of the substrate occurs, resulting in a material bond with the newly impinging droplets. As a result, the loadable area in the specimen cross-section increases. The reduction in porosity also decreases the proportion of internal pores, which has a positive effect on the tensile strengths and uniform elongations. As a result, the tensile strength and uniform strain values obtained in the tensile test increase. The enlargement of the load-bearing cross-section and the reduction of the internal notches can also be seen in the fracture surfaces recorded by scanning electron microscopy.

5. Conclusion

In this article, we investigated the influence of build platform and droplet temperatures on the properties of CuSn8 components manufactured in the MJT process. The build platform and droplet temperatures were varied in three steps using a full factorial experimental design. Optical microscopy, metallography, density determination, tensile testing, and fracture inspection were performed to analyze the properties. The following observations could be made:

- As the temperature of the droplets and the build platform increases, the height of the manufactured cuboids decreases. In addition, the number of pores on the component surface decreases.
- An increase in the temperature of the build platform and droplets causes an increase in relative component density.
- With increasing temperature of the building platform, recrystallization occurs and an increase in grain size can be observed in the material structure. In addition, the growth of the grains beyond the droplet boundaries increases.
- The mechanical properties tensile strength and uniform elongation determined in the tensile test increase with higher build platform and droplet temperature. The highest strength and elongation values are obtained at the combination of the highest droplet and build platform temperature investigated.

Coming back to our research question—“What influence do the thermal process variables droplet temperature and build platform temperature have on the quality of CuSn8 components produced in the MJT process?”—our answer is:

Both build platform and droplet temperatures affect the material jetted CuSn8 components. Increases in relative component density, tensile strength, and uniform elongation are observed with increasing droplet and build platform temperatures. In all studies, the effect of increasing the build platform temperature was more dominant than was increasing the droplet temperature. The investigations show that for the production of components with good droplet bonding, a building platform temperature close to the solidus temperature of the building material is advantageous.

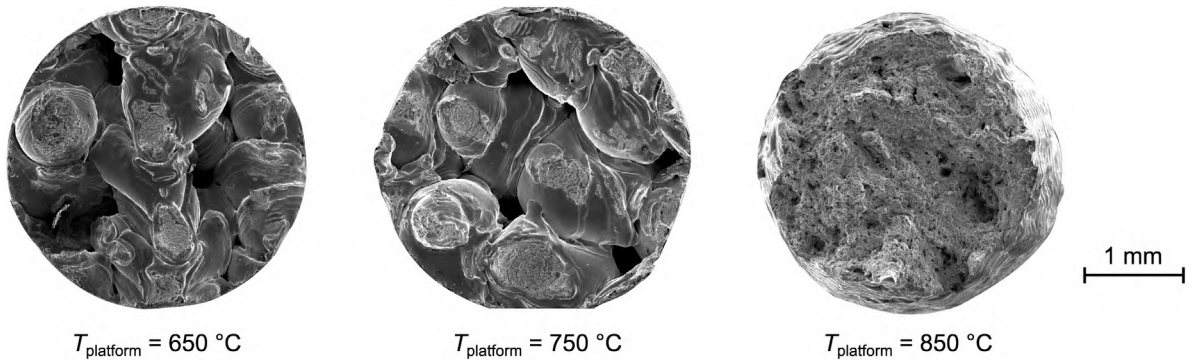


Fig. 14. Scanning electron micrographs of the fracture surfaces produced in the tensile test as a function of the platform temperature. The components were printed at a droplet temperature of 1190 °C. The build platform temperature increases from left to right from 650 °C to 850 °C. As the build platform temperature increases, the droplets fuse together better and better.

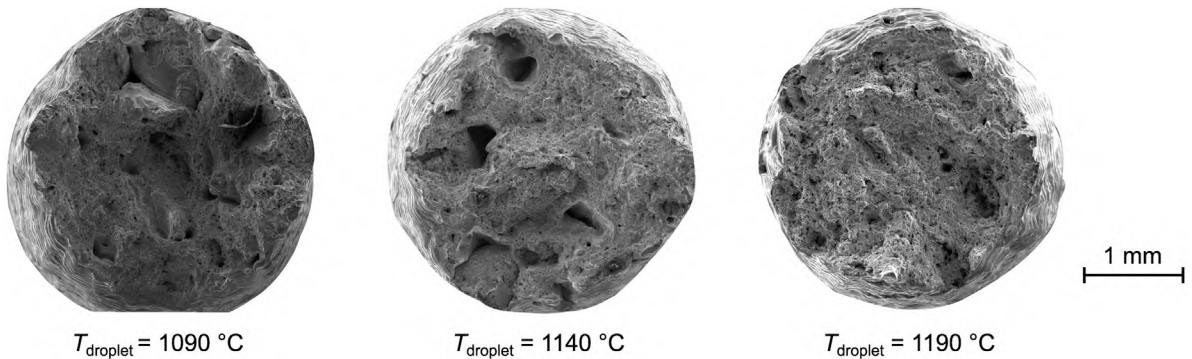


Fig. 15. Scanning electron micrographs of the fracture surfaces produced in the tensile test as a function of the droplet temperature. The components were printed at a build platform temperature of 850 °C. The droplet temperature increases from left to right from 1090 °C to 1190 °C. The increase in droplet temperature causes better fusion of the droplets with the substrate. However, the influence of the droplet temperature is less dominant compared to the build platform temperature.

CRediT authorship contribution statement

Maximilian Ploetz: Writing – original draft, Visualization, Investigation, Methodology, Writing – review & editing. **Benedikt Kirchebner:** Writing – original draft, Visualization, Investigation, Methodology, Writing – review & editing. **Wolfram Volk:** Funding acquisition, Supervision, Project administration, Writing – review & editing. **Philipp Lechner:** Funding acquisition, Supervision, Project administration, Writing – review & editing.

Declaration of competing interest

The authors declare that they have no known competing financial interests or personal relationships that could have appeared to influence the work reported in this paper.

Data availability

Data will be made available on request.

Acknowledgments

This research was supported by the Arbeitsgemeinschaft industrieller Forschungsvereinigungen (AiF, Entrepreneurial innovation) - IGF projekt-ID 21553 N and the Deutsche Forschungsgemeinschaft (DFG, German Research Foundation) - Project-ID 457434681. We would like to thank Wieland-Werke AG, for providing the semi-finished product needed to conduct this research. Furthermore, we would like to thank Corinna Sutter for her experimental support.

References

- [1] Hans Warlimont, Werner Martienssen, Springer Handbook of Materials Data, Springer International Publishing, Cham, 2018.
- [2] Joseph R. Davis (Ed.), Copper and copper alloys, ASM specialty handbook, ASM International, Materials Park, Ohio, 2001.
- [3] Christofer Leygraf, Inger Odnevall Wallinder, Johan Tidblad, Thomas Graedel, Atmospheric corrosion, second ed., The Electrochemical Society series, Wiley, Hoboken, New Jersey, 2016.
- [4] A. Alavudeen, N. Venkateshwaran, J. T. Winowlin Jappes, A Textbook of Engineering Materials and Metallurgy, Laxmi Publications, New Delhi, 2006.
- [5] Hawraa Abdulhussaien Kadhim, Iman Jabber Abed, Investigation wear behaviour of tin bronze alloy prepared by different casting techniques, IOP Conf. Ser.: Mater. Sci. Eng. 1094 (1) (2021) 012126.
- [6] Tim Mittler, Thomas Greß, Martin Feistle, Michael Krinninger, Uwe Hofmann, Joachim Riedle, Roland Golle, Wolfram Volk, Fabrication and processing of metallurgically bonded copper bimetal sheets, J. Mater. Process. Technol. 263 (3) (2019) 33–41.
- [7] Loic Constantin, Zhipeng Wu, Nan Li, Lisha Fan, Jean-François Silvain, Yong Feng Lu, Laser 3D printing of complex copper structures, Addit. Manuf. 35 (2020) 101268.
- [8] Qi Jiang, Peilei Zhang, Zhishui Yu, Haichuan Shi, Di Wu, Hua Yan, Xin Ye, Qinghua Lu, Yingtao Tian, A review on additive manufacturing of pure copper, Coatings 11 (6) (2021) 740.
- [9] C. Körner, Additive manufacturing of metallic components by selective electron beam melting — a review, Int. Mater. Rev. 61 (5) (2016) 361–377.
- [10] Yun Bai, Christopher B. Williams, An exploration of binder jetting of copper, Rapid Prototyp. J. 21 (2) (2015) 177–185.
- [11] Bonny Onuike, Bryan Heer, Amit Bandyopadhyay, Additive manufacturing of inconel 718—Copper alloy bimetallic structure using laser engineered net shaping (lens™), Addit. Manuf. 21 (May (5)) (2018) 133–140.
- [12] Jian Huang, Xingchen Yan, Cheng Chang, Yingchun Xie, Wenyu Ma, Renzhong Huang, Ruimin Zhao, Shunhua Li, Min Liu, Hanlin Liao, Pure copper components fabricated by cold spray (CS) and selective laser melting (SLM) technology, Surf. Coat. Technol. 395 (2020) 125936.
- [13] Navid Dehdari Ebrahimi, Y. Sungtaek Ju, Thermal conductivity of sintered copper samples prepared using 3D printing-compatible polymer composite filaments, Addit. Manuf. 24 (May) (2018) 479–485.

- [14] Yuchao Bai, Jiayi Zhang, Cuiling Zhao, Chaojiang Li, Hao Wang, Dual interfacial characterization and property in multi-material selective laser melting of 316L stainless steel and C52400 copper alloy, *Mater. Charact.* 167 (2020) 110489.
- [15] Linqing Liu, Di Wang, Guowei Deng, Yongqiang Yang, Jie Chen, Jinrong Tang, Yonggang Wang, Yang Liu, Xusheng Yang, Yicha Zhang, Interfacial characteristics and formation mechanisms of copper–steel multimaterial structures fabricated via laser powder bed fusion using different building strategies, *Chin. J. Mech. Eng.: Addit. Manuf. Front.* 1 (3) (2022) 100045.
- [16] Xia Lingqin, Chen Guang, Zheng Luyu, Lu Pan, Explore the feasibility of fabricating pure copper parts with low-laser energy by selective laser melting, *Mater. Res. Express* 7 (10) (2020) 106509.
- [17] S.D. Jadhav, S. Dadbakhsh, L. Goossens, J-P Kruth, J. van Humbeeck, K. Vanmeensel, Influence of selective laser melting process parameters on texture evolution in pure copper, *J. Mater. Process. Technol.* 270 (2019) 47–58.
- [18] Prashanth Konda Gokuldoss, Sri Kolla, Jürgen Eckert, Additive manufacturing processes: Selective laser melting, electron beam melting and binder jetting—Selection guidelines, *Materials* 10 (6) (2017) 672.
- [19] N.E. Gorji, R. O'Connor, D. Brabazon, XPS, SEM, AFM, and nano-indentation characterization for powder recycling within additive manufacturing process, *IOP Conf. Ser.: Mater. Sci. Eng.* 1182 (1) (2021) 012025.
- [20] Max Horn, Lena Prestel, Matthias Schmitt, Maximilian Binder, Georg Schlick, Christian Seidel, Gunther Reinhart, Multi-material additive manufacturing – Recycling of binary metal powder mixtures by screening, *Procedia CIRP* 93 (1) (2020) 50–55.
- [21] Terry Wohlers, Robert Ian Campbell, Olaf Diegel, Joseph Kowen, Noah Mostow, Wohlers report 2021: 3D printing and additive manufacturing : global state of the industry, Wohlers Associates, Fort Collins, Colorado, 2021.
- [22] Melissa Orme, Robert F. Smith, Enhanced aluminum properties by means of precise droplet deposition, *J. Manuf. Sci. Eng.* 122 (3) (2000) 484–493.
- [23] M. Fang, S. Chandra, C.B. Park, Heat transfer during deposition of molten aluminum alloy droplets to build vertical columns, *J. Mater. Process. Technol.* 131 (11) (2009) 62.
- [24] Hansong Zuo, Hejun Li, Lehua Qi, Songyi Zhong, Influence of interfacial bonding between metal droplets on tensile properties of 7075 aluminum billets by additive manufacturing technique, *J. Mater. Sci. Technol.* 32 (5) (2016) 485–488.
- [25] Wenbin Cao, Yoshinari Miyamoto, Droplet-based freeform fabrication of aluminum objects through internet, *J. Japan Soc. Powder Powder Metall.* 49 (11) (2002) 1023–1027.
- [26] Shiraz D. Aziz, Sanjeev Chandra, Impact, recoil and splashing of molten metal droplets, *Int. J. Heat Mass Transfer* 43 (16) (2000) 2841–2857.
- [27] Benedikt Kirchebner, Christoph Rehekampff, Martin Tröndle, Philipp Lechner, Wolfram Volk, Analysis of salts for use as support structure in metal material jetting, *Prod. Eng.* 15 (6) (2021) 855–862.
- [28] Song Yi Zhong, Hua Le Qi, Jun Luo, Yuan Xiao, Parameters study on generation of uniform copper droplet by pneumatic drop-on-demand technology, *Adv. Mater. Res.* 430–432 (2012) 781–784.
- [29] Song-yi Zhong, Le-hua Qi, Jun Luo, Han-song Zuo, Xiang-hui Hou, He-jun Li, Effect of process parameters on copper droplet ejecting by pneumatic drop-on-demand technology, *J. Mater. Process. Technol.* 214 (12) (2014) 3089–3097.
- [30] Benjamin Himmel, Dominik Rumschoettel, Wolfram Volk, Tensile properties of aluminium 4047a built in droplet-based metal printing, *Rapid Prototyp. J.* 25 (2) (2019) 427–432.
- [31] Johannes Schindelin, Ignacio Arganda-Carreras, Erwin Frise, Verena Kaynig, Mark Longair, Tobias Pietzsch, Stephan Preibisch, Curtis Rueden, Stephan Saalfeld, Benjamin Schmid, Jean-Yves Tinevez, Daniel James White, Volker Hartenstein, Kevin Eliceiri, Pavel Tomancak, Albert Cardona, Fiji: an open-source platform for biological-image analysis, *Nature Methods* 9 (7) (2012) 676–682.
- [32] Benjamin Himmel, Material jetting of aluminium: dissertation, Schriftenreihe Umformtechnik und Gießereiwesen, 21, TUM.University Press, Munich, 2020.